Journal of Alloys and Compounds, 194 (1993) 373–380
JALCOM 7205

Ion beam induced amorphization in the intermetallic compounds NiTi and NiAl

P. Moine and C. Jaouen
Laboratoire de Métallurgie Physique, Université de Poitiers, CNRS (U.R.A. 131), Faculté des Sciences, 40 Avenue du Recteur Pineau, F86022 Poitiers (France)

(Received December 17, 1991; in final form March 9, 1992)

Abstract

The mechanisms of ion beam induced crystal to amorphous transition in intermetallic compounds are analysed through amorphization kinetics results recently obtained from two ordered alloys, NiTi and NiAl. It is shown that the deposited energy density, which depends on the mass and the energy of the incident particle, as well as on the target, controls the transformation mechanisms. Heavy ion irradiation induces a quasi-direct amorphization in the displacement cascades, whereas damage accumulation is required when light ion is used. The influence of the material characteristics is also studied. The temperature effect on amorphous phase formation is investigated. When the temperature increases, reordering effects via radiation-enhanced diffusion processes compete with ballistic disordering so that the transformation is never complete. Finally, the influence of the amorphization kinetics on nitride precipitation in N^+ implanted NiTi alloy is discussed. At high fluences (10^{17} ions cm^{-2}) $TiN_{0.8}$ fine precipitates, embedded in an amorphous or in a crystalline matrix (depending on the temperature), are observed. These precipitates all have the same orientation, even in an amorphous matrix, when epitaxial nucleation occurs in the crystalline matrix before noticeable amorphization. They are disoriented if the nucleation starts when the amorphization is almost complete.

1. Introduction

Among all the solid-state amorphizing transformations, the crystalline to amorphous (c–a) transition, induced by high energy particle bombardment of intermetallic compounds, is one of the simplest to study: the amorphization can be followed step by step *vs.* well-controlled parameters (flux, mass and energy of the particle, substrate temperature, etc.), and is induced in a material with only metallic-type atomic bonds. As chemical disordering is often mentioned as a driving force for amorphization [1] it was appealing to compare the results of the ion irradiation induced c–a transition for two ordered alloys, the NiTi [2–9] and the NiAl [10–18], which do not present thermal chemical order–disorder transformation. The aim of this paper is to analyse, in the light of the many studies of the last decade on the subject, the mechanisms of the ion induced c–a transformation in intermetallic compounds through amorphization kinetics obtained in NiTi and NiAl alloys.

Firstly, amorphization mechanisms will be analysed and discussed with respect to the variation of amorphous volume fraction as a function of the fluence; then the temperature effect on amorphous phase formation will be presented and finally the influence of the amorphization kinetics on nitride precipitation in high fluence N^+ implanted NiTi alloy is studied.

2. Crystalline to amorphous transformation in the low temperature limit

In this section the c–a reaction is studied when the temperature is sufficiently low for the processes governing the transformation to be mainly of a ballistic nature, *i.e.* below the temperatures of interstitial and vacancy recovery stages (less than 120 K for NiAl and less than 400 K for NiTi [19]).

The most direct approach to investigating the role of irradiation on the amorphization processes is certainly by studying the dose dependence of the amorphous phase formation. Experimentally the kinetics of amorphization can be obtained from several techniques. One of the most direct is to image the amorphous zones (or the crystalline matrix) through transmission electron microscopy (TEM) dark-field (DF) images using part of the amorphous rings (or crystalline reflections). This method has been used for the NiTi c–a reaction, either through *in situ* observations of TEM samples in an

0925-8388/93/$6.00

electron microscope in line with an ion implanter [6] or through observations of TEM specimens obtained from ion implanted films electrothinned to electron transparency [3, 6, 8]. Two methods were used for NiAl studies. First, *in situ* electrical resistivity (ER) measurements were performed, using polycrystalline thin films (obtained by ion beam mixing of Ni–Al multilayers). Electrical resistivity variations are directly related to the disorder created during irradiation. Assuming that the resistivity increase resulting from amorphization is higher than the increase resulting from chemical disordering and point defect creations, the amorphous volume fraction can be deduced, as a first approximation, from a linear relationship [10–12]. Second, Rutherford backscattering (RBS) experiments associated with channelling were carried out on single NiAl crystals in order to analyse the superficial disorder of a bulk sample. The amorphous volume fraction at the maximum damage depth can be deduced from the backscattering yield

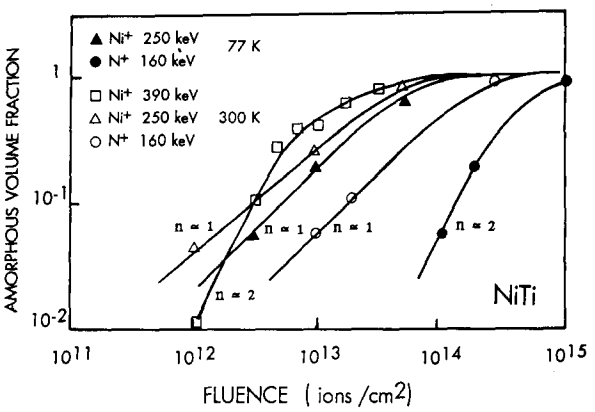

Fig. 1. Amorphous volume fraction as a function of the ion fluence, for a NiTi alloy irradiated at 77 K and 300 K with Ni and N ions (from TEM image analysis).

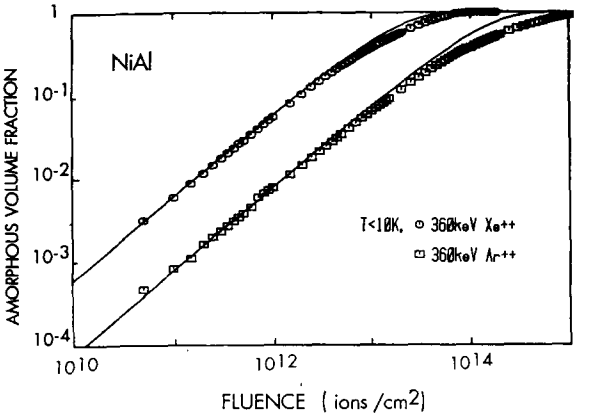

Fig. 2. Amorphous volume fraction as a function of the ion fluence for a polycrystalline NiAl film irradiated at $T < 10$ K with 360 keV Xe and Ar ions (from *in situ* resistivity measurements). The solid lines represent the best fits to experimental data, using eqn. (1) with $n = 1$.

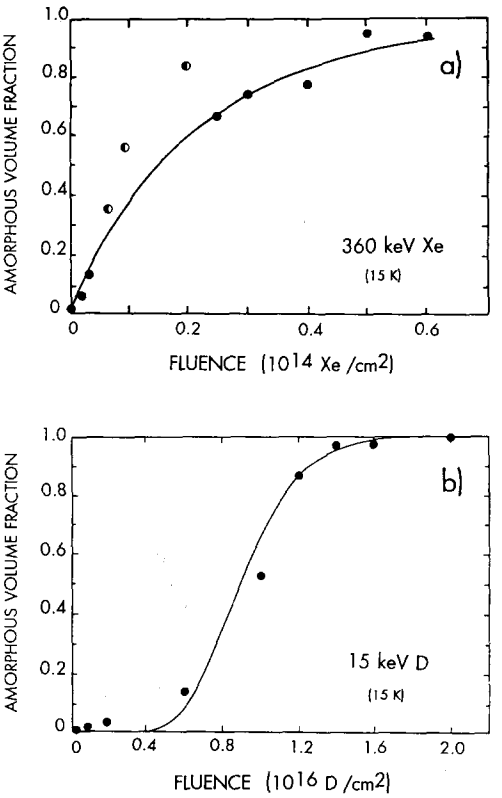

Fig. 3. Amorphous volume fraction as a function of the ion fluence for a NiAl single crystal irradiated at 15 K (from RBS experiments): (a) with 360 keV Xe^+; (b) 15 keV D^+. The solid lines represent the best fits to experimental data, using eqn. (1) with $n = 1$ and $n = 13$ respectively.

using the procedure developed in ref. 20, assuming that only disordered regions contribute to direct backscattering of the channelled fraction of analysed particles. Although TEM imaging allows the microstructural evolution to be followed directly and gives very valuable information on phase transformation, ER and RBS techniques are nevertheless of higher sensitivity for kinetic analysis of the c–a reaction. In particular, ER measurements allow a very accurate analysis at low fluences. However, owing to chemical disordering, the damage cross-sections deduced from these data are overestimated.

2.1. Experimental observations

The NiTi alloys present a martensitic transformation: the high temperature phase is a B2 structure and the martensite is a monoclinic distortion of the B19 structure [21]. For the investigated alloy, the martensitic transformation temperature is approximately 310 K. The NiAl alloy has a B2 structure over the whole temperature range.

The amorphization kinetics deduced from TEM imaging analysis are shown in Fig. 1 for the NiTi irradiated at 300 K and 77 K with Ni and N ions. The evolution

of the amorphous volume fraction C_α (deduced from ER measurements) as a function of the fluence ϕ is shown in Fig. 2 for a polycrystalline NiAl thin film irradiated with Xe and Ar ions at temperature lower than 10 K. A similar plot (deduced from RBS experiments) is shown in Fig. 3 (half-filled circles) for monocrystalline NiAl samples irradiated at 15 K with Xe and D ions.

2.2. Analysis of results and discussion

Results were analysed using Gibbon's model [22] which leads to the following relation between the amorphous volume fraction and the fluence:

$$C_\alpha = 1 - \sum_{i=0}^{n-1} \frac{(a\phi)^i}{i!} \exp(-a\phi) \quad (1)$$

The parameter a is the damage cross-section, ϕ the ion fluence and n the number of ion track overlap required for amorphization. Experimental fits to this equation give the values of a and n.

In Table 1 the irradiation characteristics and damage parameters deduced from transport of ions in matter simulations [23] are indicated, as well as the c–a transformation characteristics. The values of a for NiTi irradiation are not given because significant determination could not be achieved from experimental $C_\alpha(\phi)$ curves which were not accurate enough. Only the values of n were estimated from the slope of $C_\alpha(\phi)$ at low fluences.

2.2.1. Influence of the mass of the irradiating particle

The c–a transformation characteristics indicate that direct amorphization occurs in the core of the displacement cascade since $n \approx 1$ for a 250 keV Ni^+ irradiation of NiTi, and for a 360 keV Ar^+ or Xe^+ irradiation of NiAl. Owing to an additional formation of a premartensitic phase [16] occurring simultaneously with the amorphization, a more complicated amorphization kinetics occurs in a 360 keV Xe^+ irradiated NiAl single crystal (Fig. 3(a)). This point will be discussed later.

In the case of NiTi irradiation with 390 keV Ni^+ or 160 keV N^+ an overlap of few cascades is required for amorphization ($n \approx 2$). When a NiAl single crystal is irradiated with very light D^+ ions, the $C_\alpha(\phi)$ curves present a typical sigmoidal shape with a pronounced ion fluence threshold (Fig. 3(b)). The analysis based on Gibbon's model indicates that 13 overlaps would be necessary for amorphization ($n \approx 13$), and that the damage cross-section would be 0.14 nm^2. However, here the physical meaning of this is not very clear and other models of amorphization process, related to the statistical spatial distribution of the displaced atoms [24–26], are preferred. With this model the amorphization occurs when the concentration of defects (point defects, interstitial-vacancy complexes, antisite defects) reaches a threshold value (26).

These results show also that the energy density deposited in the displacement cascade controls the amorphization mechanism, and not only the mass of the irradiating particle. For instance, an increase of the Ni^+ ion energy from 250 keV to 390 keV, which reduces, in NiTi, the average energy density deposited in the ion track from 0.026 eV $atom^{-1}$ to 0.01 eV $atom^{-1}$, changes a direct amorphization mechanism to an overlap of two displacement cascades. Similar conclusions were deduced from c–a transition studies in the CuTi intermetallic compound [27, 28] and in the Ni_3B metal–metalloid system [25, 29].

2.2.2. Influence of the irradiated material

It must be emphasized that the displacement density required for amorphization by direct transformation

TABLE 1. Calculated irradiation parameters: η is the conversion factor from the fluence, expressed in number of ions per cm^2, to the number of displacements per atom (dpa); θ_D is the elastic energy deposited per target atom in the displacement cascade (deposited energy density) expressed in eV per atom. Damage characteristics are extracted from the fits to experimental data using eqn. (1): n represents the number of ion track overlap; a is the damage cross-section and $\nu_{0.8}$ is the dose in dpa necessary to obtain 80% of amorphous volume

System	Sample type mean grain size	T (K)	Ion	E_0 (keV)	η (dpa/ions cm^{-2})	θ_d (eV)	n	a (nm^2)	$\nu_{0.8}$ (dpa)
NiAl	Polycrystalline films	10	Xe	360	0.62×10^{-14}	0.24	$\simeq 1$	6.30	0.26
	($d \sim 20$–50 nm)	10	Ar	360	0.107×10^{-14}	2.9×10^{-2}	$\simeq 1$	0.79	0.60
NiAl	Monocrystalline	15	Xe	360	0.62×10^{-14}	0.24	$\simeq 1$	4.50	0.26
		15	D	15	0.14×10^{-16}	$<10^{-4}$	$\simeq 13$	0.14	0.16
NiTi	Polycrystalline	300	Ni	390[a]	0.4×10^{-14}	0.01	$\simeq 2$		0.10
	(d: several μm)	300	Ni	250	0.25×10^{-14}	0.026	$\simeq 1$		0.11
		77	Ni	250	0.25×10^{-14}	0.026	$\simeq 1$		0.18
		300	N	160	0.07×10^{-14}	0.6×10^{-3}	1–2		0.10
		77	N	160	0.07×10^{-14}	0.6×10^{-3}	$\simeq 2$		0.18

[a]Under an incidence of 60°.

inside the displacement cascade core, or by damage accumulation, as well as the total dose for complete amorphization, depend strongly on the system.

It is observed that the instability of the crystalline lattice to ion irradiation is larger for the NiTi than for the NiAl. This behaviour can be related to the NiTi ordering energy which is approximately twice that of the NiAl (according to Visnov's calculation [30]); as a consequence, the energy required to create antisite defects in NiTi is larger than in NiAl, so that the chemical disorder, induced by ballistic effect, reaches the amorphizing critical energy at a lower dose in NiTi than in NiAl. All of the above supports the proposition that chemical disordering is one of the driving forces for amorphization [1].

In the case of NiTi irradiation the amorphization occurs more quickly at 300 K than at 77 K for both Ni^+ and N^+ implantation. This surprising result can be explained in terms of martensite stability, since M_S is approximately equal to 310 K, so when the temperature is lowered, the martensitic state is stabilized and as a consequence the c–a transformation requires more energy at 77 K than at 300 K.

Superficial amorphization is observed at 15 K in monocrystalline NiAl samples by D^+ ion irradiation, whereas it is never observed, even at 10 K, in polycrystalline thin films irradiated with light particles [13, 16]. Again, this result shows the role of the initial structural state on the amorphization mechanism. It is thought that, in nanocrystalline films, grain boundaries are sinks for point defects and may relax the stresses induced by the volume expansion associated with the chemical disordering. As a consequence the critical point defect concentration and/or the critical stress level required for the collapse of the crystalline lattice [31, 32] would never be reached in some cases, and in particular, in NiAl polycrystalline films irradiated with light particles.

2.2.3. Martensitic transformation in an Xe^+ irradiated NiAl single crystal [15, 16]

No thermal martensitic transition is observed in the equiatomic NiAl. However, martensitic transformation occurs in Ni_xAl_{1-x} alloys. It has been shown that the linear Ni concentration dependence of the M_S temperature is such that no thermally induced martensite should be observed for alloys with a Ni concentration smaller than 60 at.% [33].

However, *in-situ* TEM observations during Xe^+ irradiation performed at 10 K, of a NiAl single crystal, reveal the formation of a premartensitic phase, simultaneous with amorphization; for larger fluences this premartensite phase reverts to the original B2 phase (Fig. 4) [15] before complete amorphization. This complex phase transformation can explain the variation (as a function of the fluence) of the disordered volume fraction deduced from the measurements of the aligned RBS yield (Fig. 3(a)) [16]. At low ion fluences (less than 2.10^{13} Xe^+ cm^{-2}) the initial increase of the aligned RBS yield can be partly correlated to the formation of a martensitic phase (Fig. 4(b)), induced by strong compressive stresses created by amorphous and disordered regions formed inside the displacement cascade core. As the Xe^+ fluence increases, the aligned backscattering yield decreases. This effect is related to the reversion of the martensitic phase to the initial ordered B2 structure (or partially disordered). Martensite reflections disappear in the electron diffraction patterns (Fig. 4(c)). Beyond 2.5 10^{13} Xe^+ cm^{-2} the aligned RBS yield increases again, whereas, in electron diffraction pattern, diffuse rings grow, corresponding to amorphous phase, indicating that the B2 structure transforms to amorphous. This crystalline phase sequence transformation (martensite ⇒ B2 ⇒ partially disordered B2 ⇒ amorphous) is similar to that observed in electron irradiated NiTi [6].

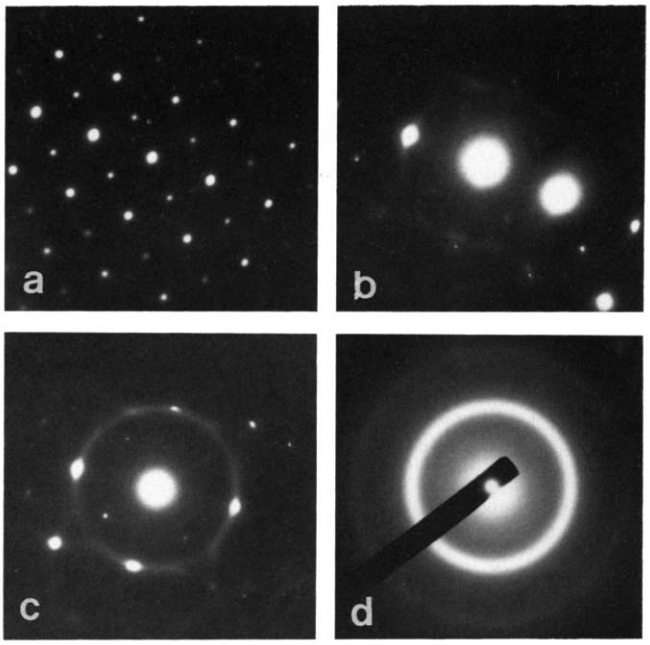

Fig. 4. [001] zone axis, SADPs from a NiAl sample irradiated at 10 K with 360 keV Xe^+: (a) before irradiation; (b) after a fluence of 10^{13} Xe^+ cm^{-2}; (c) after a fluence of 3×10^{13} Xe^+ cm^{-2}; (d) after a fluence of 10^{14} Xe^+ ions cm^{-2}. In (b) streaks and premartensitic reflections are visible whereas the intensity of the superlattice spots of the matrix decrease. In (c) diffuse ring begins to appear whereas at the same time the streaks and extra spots disappear. In (d) only diffuse rings are present.

3. Temperature dependence

3.1. Experimental observations

3.1.1. 360 keV Xe^+ irradiation in NiAl [11, 17, 18]

From resistivity measurements, the evolution of the amorphous volume fraction C_α as a function of ion

fluence ϕ is shown in Fig. 5 for different temperatures from 4 to 300 K. At low fluences, the c–a reaction kinetics are all compatible with a direct damage mechanism since a linear dependence of C *vs.* ϕ is observed. These kinetics are quite similar between 4 and 77 K, but the fluence required for complete amorphization sharply increases between 77 and 120 K and beyond this temperature complete amorphization cannot be obtained. The variation of C_L, the amorphous volume fraction at saturation, *vs.* the temperature T is shown in Fig. 6. The temperature dependence of the total dose for ion induced amorphization is shown in Fig. 7(a). In the same figure, the temperature dependence of the required dose for a complete ion induced crystallization of the amorphous state is also indicated.

3.1.2. 250 keV Ni^+ irradiation in NiTi [6, 8]

From TEM image analysis, the evolutions of the amorphous volume fraction as a function of ion fluence ϕ were shown in Fig. 1 for two temperatures, 77 and 293 K, and the results were discussed above. Crystalline–amorphous reaction kinetics have not been carried out for other temperatures but the amorphous volume fraction at saturation, C_L, has been determined

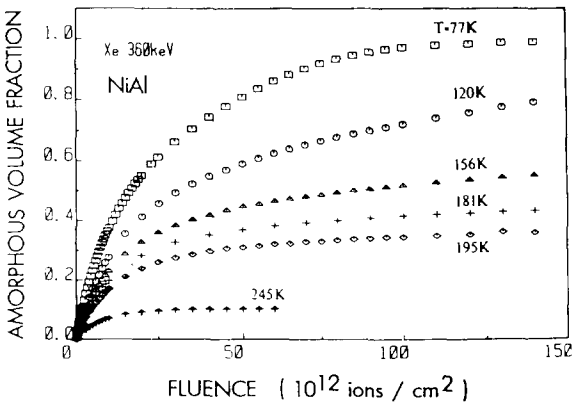

Fig. 5. Amorphous volume fraction as a function of the ion fluence for different temperatures from 77–300 K for a 360 keV Xe^+ NiAl irradiation.

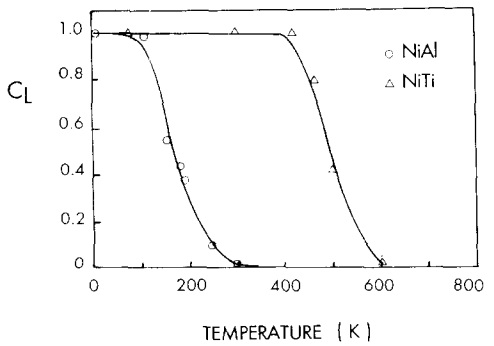

Fig. 6. Amorphous fraction at saturation, C_L, as a function of the temperature for a 360 keV Xe^+ irradiated NiAl and a 250 keV Ni^+ irradiated NiTi.

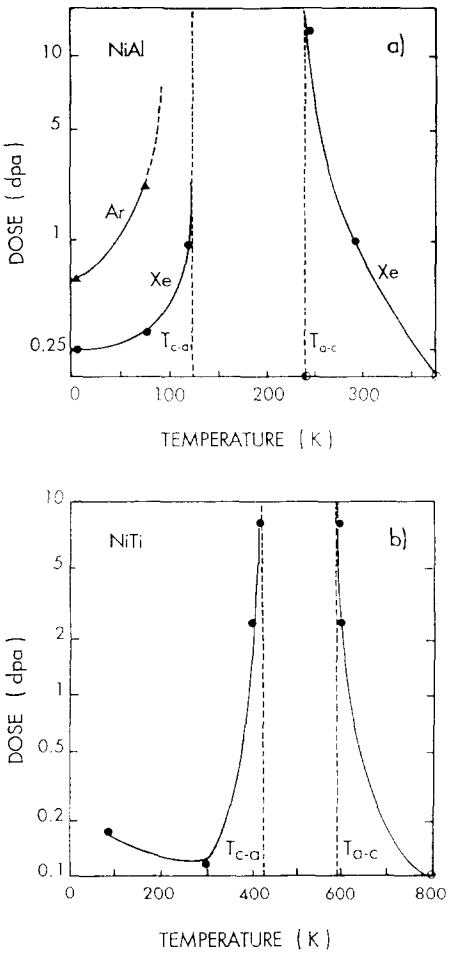

Fig. 7. Total dose for ion irradiation induced amorphization of the crystalline state and for ion induced crystallization of the amorphous state, as a function of the temperature: (a) for a 360 keV Xe^+ and 360 keV Ar^+ irradiated NiAl; (b) for a 250 keV Ni^+ irradiated NiTi. T_{c-a} is the limit temperature above which the amorphization of the crystalline state is never complete. T_{a-c} is the limit temperature below which the crystallization of the amorphous state is never complete.

for 77, 300, 420, 500, 570 and 600 K. The graph $C_L(T)$ for NiTi is shown in Fig. 6.

The temperature dependence of total dose for ion induced amorphization, as well as that of the required dose for a complete ion induced crystallization of the amorphous state, is shown in Fig. 7(b).

3.2. Results analysis

In both cases there is a critical temperature T_{c-a}, (120 K for NiAl and 425 K for NiTi), above which amorphization cannot be complete. In the temperature range 120–240 K for NiAl and 425–600 K for NiTi the amorphous volume fraction at saturation decreases from 1 to 0. These temperature ranges are lower than the minimum temperature T_{a-c} for ion induced homogeneous crystallization (240 K for NiAl and 600 K for NiTi) (see Figs. 6, 7). This behaviour suggests that

there is a competition between ballistic disordering mechanisms, inducing amorphization, and a reordering process, leading to crystallization. As this happens in a temperature range where crystalline nucleation into the amorphous phase cannot occur, even under irradiation (see Fig. 7), it is suggested [11, 17, 18] that the reordering effects correspond to crystalline growth via interfaces between amorphous zones and the crystalline matrix. This process does not occur in the same temperature range for the NiAl and for the NiTi, but it corresponds in both cases to the interstitial recovery stage [19].

4. Influence of amorphization kinetics on precipitation in N^+ implanted NiTi

4.1. Experimental observations [7–9]

Implantation of 160 keV N^+ has been performed in NiTi, at 77, 300, 380, 480 and 580 K, for large fluences (10^{17} ions cm^{-2}). The average N^+ concentration in the TEM thin film is approximately 4 at.% for a fluence of 10^{17} ions cm^{-2}. X-ray photoelectron spectroscopy study [7] indicates that the precipitates are $TiN_{0.8}$. Whatever the temperature, a very fine precipitation of titanium nitrides is observed, inside an amorphous matrix until $T=380$ K and inside a crystalline matrix for $T>380$ K.

At 77 K selected area diffraction patterns show diffuse amorphous rings and a periodic lattice of reflections which light, in d.f. images, small particles (about 25 nm in size), embedded in an amorphous layer (Fig. 8(a)). It is deduced that these precipitates all have the same orientation.

At 300 K and 380 K SADPs show together halo rings and dotted rings. These features indicate that the tiny precipitates (about 10 nm in size), (lit by part of the dotted rings in d.f. images), are disoriented inside an amorphous matrix (Fig. 8(b)).

At 480 K the partially amorphized matrix includes small oriented precipitates in epitaxy with the matrix (Fig. 8(c)). The SADPs show amorphous NiTi diffuse rings and spots characteristic of the crystalline NiTi and of TiN precipitates. At 580 K and above there is no further amorphization but a fine precipitation in epitaxy with the matrix (Fig. 8(d)). The epitaxial relationships are: $(011)_{TiN} \| (001)_{NiTi}$ and $[200]_{TiN} \| [200]_{NiTi}$ [7].

4.2. Results analysis

To explain the orientation of the precipitates embedded in the amorphous matrix at 77 and 480 K and their disorientation at 300 and 380 K the following mechanism is proposed. When TiN nucleation occurs before amorphization, precipitates form in epitaxy with the crystalline matrix; further ion irradiation induces amorphization of the matrix, but does not affect the crystalline structure and the orientation of the precipitates. If the amorphization occurs before nucleation, precipitates formed in an amorphous layer are disoriented.

As noticeable amorphization occurs for a larger dose at 77 K than at 300 K (6.10^{14} ions cm^{-2} against 2.10^{14} ions cm^{-2}, for 10% of amorphous volume fraction), it can be assumed that, at 77 K, epitaxial nitride precipitates form in a crystalline matrix before its amorphization, whereas at 300 K they form an amorphous matrix. As a consequence the precipitates will be oriented in the amorphous layer at 77 K and disoriented at 300 K. At 480 K, the competition between ballistic disordering and crystallization through crystalline matrix–amorphous zone interface delays the amorphization and allows the nucleation of epitaxial nitrides: the precipitates are reoriented. From these experiments it can be estimated that the critical fluence for nitride nucleation corresponds to that for which the amorphization is almost complete at 77 K and just noticeable at 300 K. This critical fluence, determined from Fig. 1, is approximately 10^{14} N^+ ions cm^{-2} corresponding to an average atomic nitride concentration of 4×10^{-5}, in the implanted NiTi layer. These experiments show also that, even at low temperature (77 K), nitride nucleation can occur, and that nitride precipitates can grow inside the amorphous phase through an enhanced diffusion associated with implantation defects.

5. Conclusion

These studies confirm that ion beam induced amorphization depends on irradiation parameters through the deposited energy density, and also on the material microstructural characteristics. In particular, it was seen that chemical disordering energy, phase stability, ion irradiation induced phase transformation and grain size could greatly affect the mechanisms in question.

Beyond a critical irradiation temperature, amorphization cannot be complete because of competition between ballistic disordering and ion induced reordering. As this occurs in a temperature range where no crystallization can happen, even under ion irradiation, diffusion through amorphous–crystal interfaces is assumed.

In the particular case of NiTi alloys, N^+ implantation with large fluences induces nitride precipitation and amorphization. These precipitates are oriented if nucleation occurs before noticeable amorphization and disoriented if the amorphization is almost complete before the precipitation starts. This demonstrates that,

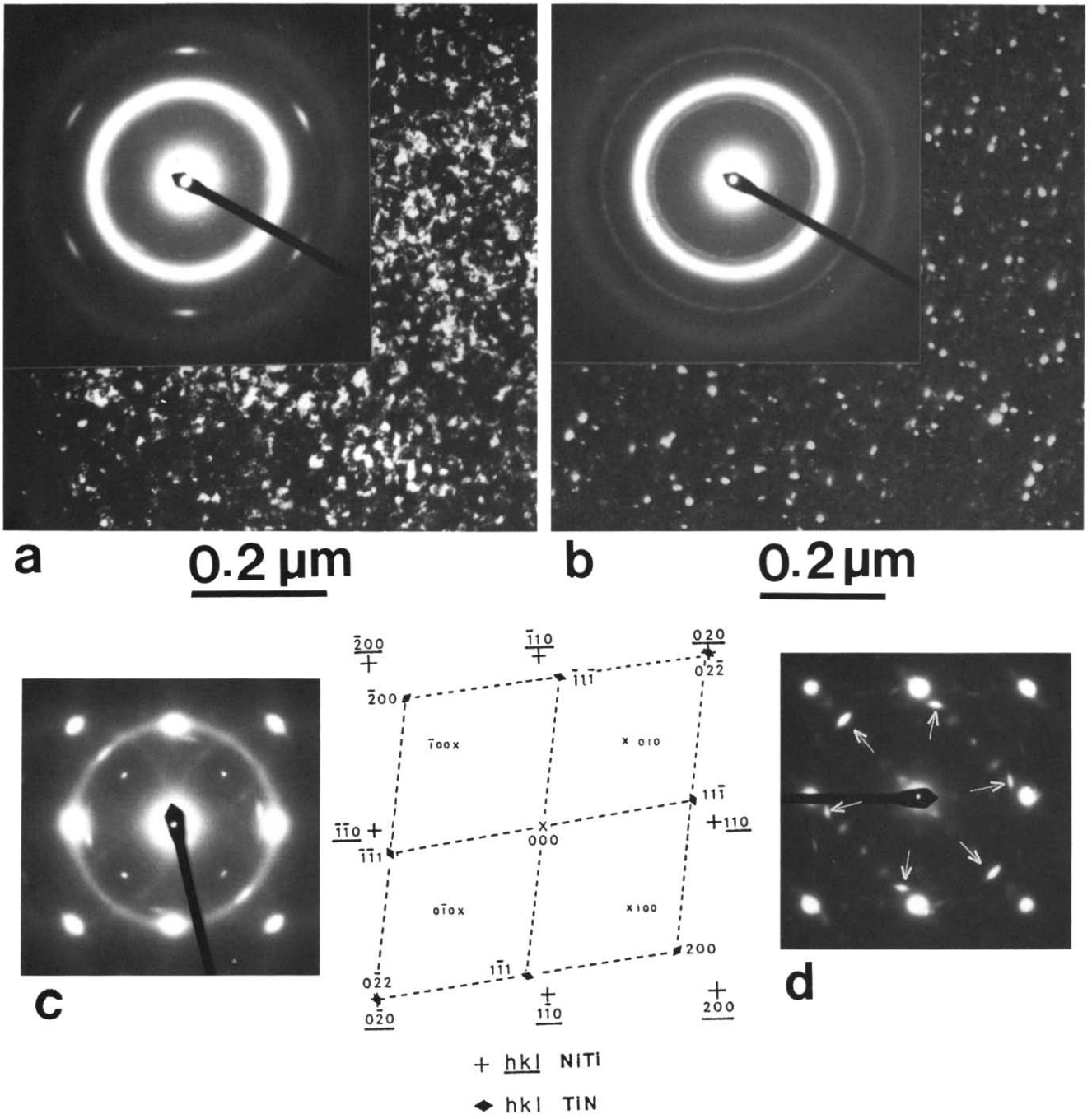

Fig. 8. 160 keV N^+ implanted NiTi with a fluence of 10^{17} ions cm^{-2}: (a) at 77 K: SADP and d.f. image taken with one of the extra reflections, lighting oriented nitride precipitates; (b) at 300 K: SADP and d.f. image taken with a part of the dotted rings, lighting disoriented nitride precipitates; (c) at 480 K: SADP showing NiTi diffuse amorphous ring, NiTi (B2) reflections and epitaxial nitride spots in a [100]NiTi zone axis, as schematically explained; (d) at 580 K: SADP showing NiTi crystalline reflections and epitaxial nitride spots (indicated by arrows) in a [100]NiTi zone axis.

even at low temperature, nucleation and growth can occur, through a radiation-enhanced diffusion process.

References

1 D. E. Luzzi, H. Mori, H. Fujita and M. Meshii, *Acta Metall., 34* (1986) 629.

2 P. Moine, J. P. Rivière, N. Junqua and J. Delafond, *Proc. Mater. Res. Soc., 7* (1982) 243.

3 J. L. Brimhall, H. E. Kissinger and L. A. Charlot, *Proc. Mater. Res. Soc., 7* (1982) 235.

4 P. Moine, J. P. Eymery, R. J. Gaboriaud and J. Delafond, *Nucl. Instrum. Methods, 209/210* (1983) 267.

5 J. M. Brimhall, H. E. Kissinger and A. R. Pelton, *Proc. Mater. Res. Soc., 27* (1983) 163.

6 P. Moine, J. P. Rivière, M. O. Ruault, J. Chaumont, A. R. Pelton and R. Sinclair, *Nucl. Instrum. Methods B, 7/8* (1985) 20.
7 O. Popoola, M. F. Denanot, P. Moine, J. P. Villain, M. Cahoreau and J. Caisso, *Acta Metall., 37* (3) (1989) 867.
8 J. Delage, O. Popoola, J. P. Villain and P. Moine, *Mater. Sci. Eng. A, 115* (1989) 133.
9 J. Delage, Ph.D. Thesis, *Amorphisation induite par faisceau d'ions dans le système Ni–Ti,* Poitiers, 1989.
10 C. Jaouen, J. P. Rivière, R. J. Gaboriaud and J. Delafond, *Amorphous Metals and Non Equilibrium Processing,* Les éditions de Physique, Paris, 1984, p. 117.
11 C. Jaouen, Thèse d'Etat, Poitiers, 1987.
12 C. Jaouen, J. Delafond and J. P. Rivière, *J. Phys. F, 17* (1987) 335.
13 J. P. Rivière, C. Jaouen and J. Delafond, *Mater. Sci. Forum, 15/18* (1987) 111.
14 L. Thomé, C. Jaouen, J. P. Rivière and J. Delafond, *Nucl. Instrum. Methods B, 19/20* (1987) 554.
15 C. Jaouen, M. O. Ruault, H. Bernas, J. P. Rivière and J. Delafond, *Europhys. Lett., 4* (9) (1987) 1031.
16 C. Jaouen, J. P. Rivière, J. Delafond, L. Thomé, F. Pons, R. Danielou, J. Fontenille and E. Ligeon, *J. Appl. Phys., 65* (1989) 1499.
17 C. Jaouen, J. P. Rivière and J. Delafond, *Nucl. Instrum. Methods B, 59/60* (1991) 406.
18 C. Jaouen, in G. Martin and L. Kubin (eds.), *Non Linear Phenomena in Materials Science,* Trans. Tech. Publ., 1992, p. 123.
19 J. P. Rivière, personal communication, 1986.
20 A. Benyagoub and L. Thomé, *Radiat. Eff. 105* (1987) 9.
21 G. M. Michal and R. Sinclair, *Acta Crystallogr. B37* (1981) 1803.
22 J. F. Gibbons, *Proc. IEEE, 60* (1972) 1062.
23 J. F. Ziegler, J. P. Biersack and V. Littmark, *The Stopping and Range of Ions in Solids,* Pergamon, New York, 1986.
24 E. P. Simonen, *Nucl. Instrum. Methods B, 16* (1986) 198.
25 A. Benyagoub and L. Thomé, *Phys. Rev. B, 38* (1988) 10205.
26 D. F. Pedrazza, *J. Mater. Res. 1* (1986) 425.
27 J. Koike, P. R. Okamoto and M. Meshii, *J. Non-Cryst. Solids, 106* (1988) 230.
28 J. Koike, P. R. Okamoto, L. E. Rehn and M. Meshii, *J. Mater. Res., 4* (1989) 1143.
29 L. Thomé, F. Pons, E. Ligeon, J. Fontenille and R. Danielou, *J. Appl. Phys., 63* (1982) 722.
30 R. Visnov, J. A. Alonso and L. A. Girifalco, *Metall. Trans. A, 11* (1980) 1747.
31 G. Linker, *Mater. Sci. Eng., 69* (1985) 105.
32 P. R. Okamoto, L. E. Rehn, J. Pearson, R. Bhadra and M. Grimsditch, *J. Less-Common Met., 140* (1988) 231.
33 J. L. Mialek and R. F. Heheman, *Metall. Trans., 4* (1973) 1571.